Journal of Applied Physics

RESEARCH ARTICLE | SEPTEMBER 19 2024

Piezo-photocatalysis synergy in γ-GeSe for highly efficient oxygen evolution reaction

Tianqi Zhang ; Long Zhou ; Guobo Chen; Songrui Wei ; Rong Sun; Yunping Li ; Lijian Meng ; Guanglong Zhang ; Shuwei Xia ; Zhongchang Wang ; Meng Qiu

J. Appl. Phys. 136, 114302 (2024)
https://doi.org/10.1063/5.0217893

AIP Publishing

Journal of Applied Physics ARTICLE pubs.aip.org/aip/jap

Piezo-photocatalysis synergy in γ-GeSe for highly efficient oxygen evolution reaction

Cite as: J. Appl. Phys. **136**, 114302 (2024); doi: 10.1063/5.0217893
Submitted: 7 May 2024 · Accepted: 31 August 2024 ·
Published Online: 19 September 2024

Tianqi Zhang,[1,2] Long Zhou,[1] Guobo Chen,[1] Songrui Wei,[3] Rong Sun,[2] Yunping Li,[4] Lijian Meng,[5] Guanglong Zhang,[6,a)] Shuwei Xia,[1,a)] Zhongchang Wang,[2,7,a)] and Meng Qiu[1,a)]

AFFILIATIONS

[1]Key Laboratory of Marine Chemistry Theory and Technology (Ocean University of China), Ministry of Education, Qingdao 266100, China
[2]International Iberian Nanotechnology Laboratory (INL), Braga 4715-330, Portugal
[3]Interdisciplinary Center of High Magnetic Field Physics of Shenzhen University, College of Physics and Optoelectronic Engineering, Shenzhen University, Shenzhen 518060, China
[4]State Key Lab for Powder Metallurgy, Central South University, Changsha 410083, China
[5]CIETI, ISEP, Polytechnic of Porto, Rua Sr. António Bernardino de Almeida, Porto 4249-015, Portugal
[6]State Key Laboratory for Marine Corrosion and Protection, Luoyang Ship Material Research Institute, Qingdao 266100, China
[7]School of Chemistry, Beihang University, Beijing 100191, China

[a)]Authors to whom correspondence should be addressed: glzhang98@163.com; shuweixia@ouc.edu.cn; zhongchangwang@buaa.edu.cn; and mengqiu@ouc.edu.cn

ABSTRACT

Solar-driven semiconductor photocatalysts are highly appealing in applications of environmental remediation and energy conversion. However, photocatalytic reactions, particularly oxygen evolution reaction (OER), are often constrained by the swift recombination of electron–hole pairs, thereby resulting in low reaction efficiency. Although it is effective to separate charge carriers by constructing heterojunctions to form built-in electric field, the lattice mismatch and inefficient interlayer charge transfer of heterojunctions in the photocatalysts limit their further development. Here, we propose a new strategy by constructing an internal electric field for OER through an individual piezoelectric two-dimensional material. The results indicate that the piezoelectric effect regulates the electronic structure, reduces bandgap, improves light absorption efficiency, and that the displacement of positive and negative charge centers is the key factor in the enhanced OER. This research indicates the feasibility of combining piezoelectric properties of two-dimensional materials with OER (1.19 eV), providing new insights and guidance for applying the piezoelectric effect in the OER and opening up a way to promote efficient separation of charge carriers.

I. INTRODUCTION

Semiconductor catalysis has been regarded as a highly promising approach to overcome the present and future energy and environmental challenges.[1] Ever since the discovery of water-splitting upon titanium dioxide (TiO_2) under light irradiation,[2] numerous semiconductor materials have been extensively investigated.[3] However, there still exist obvious drawbacks, such as low solar energy utilization and photocatalytic efficiency, especially low solar-to-hydrogen (STH) efficiency, thereby limiting further development of photocatalytic systems.[4] The low photocatalytic efficiency is mainly attributed to the inherent recombination of carriers.[5–9] Numerous strategies have been proposed to address this issue, including the optimization of model design, doping, and heterojunctions.[5] Recently, the Z-scheme heterojunctions have attracted widespread attention due to their ability to generate built-in electric fields that can fulfil electron–hole separation and possess strong redox potentials.[10] However, seeking a proper material to construct Z-scheme heterojunction remains difficult,[10] rendering it indispensable to single out two materials with matching band structures and work functions as well as lattice mismatch of

less than 5%. Thus, exploring alternative heterojunctions is expected to optimize process efficiency and lower costs.

Piezoelectric materials may serve as a candidate in terms of constructing efficient internal electric fields to separate charge.[11–16] Hong *et al.* reported direct conversion of mechanical energy into chemical energy by applying piezoelectricity of chemical catalysis (PZEC) and fulfilled photocatalytic water-splitting by piezoelectric technology.[17] Wu *et al.* utilized $BaTiO_3$ nanowires as a model system to elucidate the piezocatalytic catalytic mechanism.[18] They found that piezoelectricity causes charge centers of $BaTiO_3$ to shift along the polar axis, producing piezoelectric potential, which enhances the piezoelectric catalytic activity of $BaTiO_3$ in opposite directions. Such piezoelectric technology holds promise in developing next-generation catalysts. Traditional piezoelectric materials are often three-dimensional (e.g., $BaTiO_3$), which have issues of poor conductivity, brittleness, easy fracture, and difficulty in integration due to their large dimension, severely limiting their applications. On the other hand, two-dimensional (2D) materials show flexibility and bendability, which are applicable for flexible electronic devices and wearable technology. In addition, due to their sheet nanostructures, they can be integrated with other 2D materials to form 2D heterostructures, thereby extending their application fields.[19] Decades after the successful peeling of graphene,[20] 2D nanosheets have attracted significant attention due to their favorable characteristics, e.g., high surface-to-volume ratio, relatively short carrier migration distance, and abundant active sites.[21–23] A considerable group of 2D materials have been found to show exceptional catalytic capability, such as transition metal dichalcogenides (TMDs), transition metal carbides/nitrides (MXenes), and black phosphorus (BP).[6] Nevertheless, their practical application as a photocatalyst is still impeded by the issue of carrier recombination.[24,25]

Previous studies reported that the freestanding honeycomb-like γ-GeSe, which acts as a representative 2D ferroelectric material, is structurally stable.[26,27] Liu *et al.* found that both ferroelectricity and the induced ferromagnetism are tunable by strain. Such behaviors indicate that γ-GeSe may exhibit great potential in microelectronics and spintronics. They also demonstrated that the monolayered γ-GeSe is a 2D ferroelectric material with an out-of-plane polarization of $\sim 6.48 \times 10^{-12}$ C/m.

Despite the growing interest in piezoelectric materials, most study on two-dimensional piezoelectric materials has concentrated on experimental verification, with insufficient focus on their intrinsic mechanisms. Since 2007, numerous experiments have successfully synthesized piezoelectric materials and applied them across various fields. However, there is a lack of detailed mechanistic understanding of how these piezoelectric materials specifically drive photocatalysis.[28,29] We propose a strategy to enhance the built-in electric field of ferroelectric materials by strain to promote the photocatalytic performance of γ-GeSe and explain the mechanism in detail. Here, we found that piezoelectric materials are responsible for generating a built-in electric field through the offset of positive and negative charge centers, thereby driving the separation of electrons and holes, replacing the Z-scheme heterojunctions. This proposes a theoretical basis for utilizing a single piezoelectric material instead of constructing complex heterojunctions, hence simplifying and reducing the cost of the catalyst production process. Furthermore, most research on the piezoelectric effect has focused on photocatalytic hydrogen evolution reaction. It remains inadequate research on its application in oxygen evolution reaction (OER).[30,31] Here, we conducted a detailed analysis of polarization intensity, carrier mobility, and charge differential density to elucidate the mechanism through which the piezoelectric effect enhances electron–hole separation. Our study identifies the fundamental mechanism by which the piezoelectric effect enhances OER performance and provides theoretical support for its application in OER. We found an optimal OER barrier of 1.19 eV is obtained under 8% strain. The findings of using simple piezoelectric materials to generate built-in electric fields to promote charge separation for OER open up a promising way to extend application area of other inert materials for electrocatalytic applications.

II. COMPUTATIONAL METHODOLOGY

Density functional theory (DFT) calculations were performed with the Vienna *ab initio* simulation package (VASP).[32] The generalized gradient approximation of the Perdew–Burke–Ernzerhof (GGA-PBE)[33] exchange–correlation functional was adopted to describe the electronic structures of the system. Since the GGA method usually underestimated bandgaps of semiconductors, the Heyd–Scuseria–Ernzerhof hybrid functional (HSE06)[34,35] method was adopted to acquire more accurate band structures and optical properties. A vacuum layer of 15 Å was adopted to eliminate spurious interactions between adjacent layers. The plane-wave energy cut-off, forces, and energy difference criteria were set as 500 eV, 0.01 eV/Å, and 10^{-5} eV, respectively. The Berry phase method[36] was used to calculate electric polarization. The modern theory of polarization based on Berry's phase approximation was[36,37] used to calculate the piezoelectric stress coefficient e_{ij}. The relaxed-ion elastic and piezoelectric tensors were obtained as a sum of ionic and electronic contributions,[38]

$$C_{ijkl} = \frac{d_{ij}}{d_{kl}} = C^{ion}_{ijkl} + C^{el}_{ijkl}, \tag{1}$$

$$e_{ijk} = \frac{dP_i}{d_{jk}}, \tag{2}$$

$$d_{ijk} = \frac{dP_i}{d_{jk}}, \tag{3}$$

where $_{ij}$, $_{jk}$, and P_i are stress tensor, strain tensor, and polarization, respectively. The polarization components of the polarization tensor P_i along along x, y, and z were indicated by the subscripts $i = 1$, 2, and 3, respectively. By applying the Voigt notation, e_{ijk} and d_{ijk} were reduced to e_{il} and d_{il}, respectively. DFT simulations were employed to calculate the piezoelectric coefficients of e_{il} and d_{il} using the following expression:

$$e_{il} = d_{ik}C_{kl} \tag{4}$$

The piezoelectric coefficient of the P3m1 space group could be simplified as e_{11}, $e_{31,}$ and d_{11}, d_{31}. Based on the definition of stress–strain, the piezoelectric coefficient could be obtained by the

following formula:[39]

$$d_{11} = \frac{e_{11}}{C_{11} - C_{12}}, \tag{5}$$

$$d_{31} = \frac{e_{31}}{C_{11} + C_{12}}. \tag{6}$$

The first Brillouin zone was sampled using a G-centered $7 \times 7 \times 1$ grid for geometrical optimization and $11 \times 11 \times 1$ for electronic properties. A four proton-coupled electron-transfer (PCET) process at standard conditions ($T = 298$ K, P = 1 bar, pH = 0)[40] was adopted to evaluate the potential of the piezoelectricity induced catalytic performance,

$$^{*} + H_2O \rightarrow OH^{*} + H^{+} + e^{-}, \tag{7}$$

$$OH^{*} \rightarrow O^{*} + H^{+} + e^{-}, \tag{8}$$

$$O^{*} + H_2O \rightarrow OOH^{*} + H^{+} + e^{-}, \tag{9}$$

$$OOH^{*} \rightarrow + O_2 + H^{+} + e^{-}, \tag{10}$$

where the symbol * represents the reaction site on the substrate surface, and O*, OH*, and OOH* standfor the adsorbed oxygen, hydroxyl, and hydroperoxy groups, respectively. The step with maximum Gibbs free energy change (ΔG) of these four steps was the potential determining step. To estimate the potential determining step, the Gibbs free energy change (ΔG) of each chemical reaction was calculated by

$$\Delta G(U,\ pH,\ T) = \Delta E + \Delta ZEP - T\Delta S + \Delta G_U + \Delta G_{pH}, \tag{11}$$

where ΔE is the reaction energy determined from the calculated total energies by DFT, ΔZEP is the difference in zero-point energy, and ΔS is the change in entropy taken from the standard tables for gas-phase molecules.

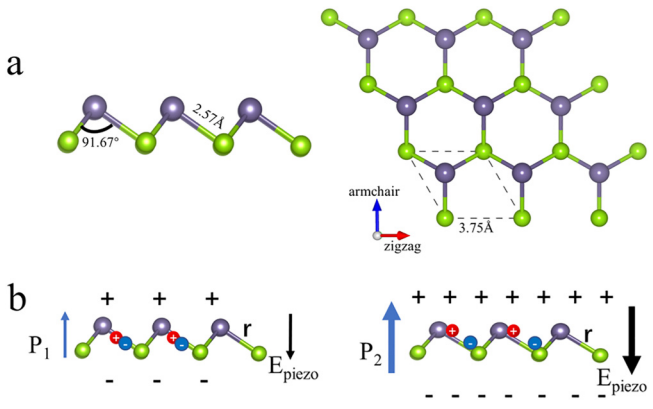

FIG. 1. Monolayered γ-GeSe with a buckled honeycomb structure. (a) Top and side view of the atomic configuration of the γ-GeSe phase. (b) Schematic illustration of piezoelectricity.

TABLE I. Lattice parameters (Å), bond length (Å), and bandgaps (eV) of γ-GeSe and other work.

	Lattice constant (Å)	Bond length (Å)	Bandgap (eV)
Calculate	3.57	2.57	3.02
Ref. 1[41]	3.62	2.55	…
Ref. 2[27]	3.67	…	3.07
Ref. 3[26]	3.68	2.57	…
Ref. 4[42]	3.66	…	3.00

III. RESULTS AND DISCUSSION

A. Structure and stability of γ-GeSe

Similar to silicene, γ-GeSe takes a buckled hexagonal lattice. After optimization (Fig. 1), it still keeps a hexagonal structure with $a = b = 3.57$ Å and a bond length (d_{Ge-Se}) of 2.57 Å, close to the values of previous theoretical calculation (3.67 Å, 2.57 Å),[27] which verified the accuracy of our calculation (Table I). The cohesive energies of γ-GeSe are calculated to be 4.02 eV, in good accordance with previous results.[26]

Ab initio molecular dynamics (AIMD) calculations and phonon spectrum analysis were utilized to assess their stabilities. As shown in Fig. S1 in the supplementary material, geometric structures do not show significant changes within 20 ps, indicating that these γ-GeSe are thermally stable. According to the phonon dispersion (Fig. S2 in the supplementary material), except for some negligible imaginary modes near the G point, all structures exhibited positive modes in the whole first brillouin zone, indicating the excellent stability of the system. In addition, the stability of γ-GeSe was also assessed by the phonon dispersion calculation[26] and *ab initio* molecular dynamic (AIMD) simulations in a previous study.[27] These calculations indicate the stability of the γ-GeSe monolayer.

B. Piezoelectric properties of γ-GeSe

As a typical two-dimensional ferroelectric material, the buckled structure of γ-GeSe disrupts the spatial inversion symmetry, leading to spontaneous polarization.[27] According to the Berry phase theory (zero electric field), polarization between any two-crystal states corresponds to a geometric phase. This theory has been successfully adopted to calculate changes in macroscopic polarization and used to study the phenomenon of spontaneous polarization. The electric polarization can be divided into ion polarization and electron polarization.[36]

The piezoelectric coefficient is given in Table S1 in the supplementary material, indicating that γ-GeSe has a remarkably higher piezoelectric coefficient than the typical 2D piezoelectric materials such as MoS_2, PN, AsN, and AsP,[38] indicating that γ-GeSe is a piezoelectric material with excellent performance. We also compared γ-GeSe with other 2D materials of the same space group (Table S1 in the supplementary material). Our calculated

piezoelectric coefficient of γ-GeSe is 49.75 pm/V, indicating that it is a promising piezoelectric material since semiconductors exhibit excellent piezoelectric properties as their piezoelectric coefficient is in the range of 6.94–243.45 pm/V.[28]

Figure 1(b) shows the principle of piezoelectricity shown in Fig. 1(b), where strain causes the shift of off-centering displacement (r_i) of Ge and Se, resulting in polarization change. The spontaneous out-of-plane electric polarization of the γ-GeSe monolayer is calculated to be 6.8×10^{-12} C/m, in line with the previously reported data.[27] Such electric polarization is attributed to the variation in the off-centered displacement between Ge and Se atoms, which induces changes in ion polarization, thereby altering the polarization intensity. The piezoelectric effect arises from the displacement of charge centers within a crystal lattice when subjected to mechanical strain. According to the equation of the electric dipole moment formula,

$$P = \sum_{i=1}^{N} q_i(r_i' - r)\,, \tag{12}$$

where P is the electric dipole moment, q is the magnitude of the charge, and r is the central location, r_i' is the center of positive and negative charges. Strain increases the magnitude of r_i', thereby increasing the electric dipole moment and increasing the polarization strength. We speculate that the external strain on γ-GeSe by modifying d_{Ge-Se} would consequently impose impact on polarization intensity leading to obvious piezoelectric effect, and thus further on the magnitude of the built-in electric field.

Since 2D materials are flexible, they could withstand deformation of less than 10% before rupture.[43] To explore the impact of strain on polarization intensity of γ-GeSe, we implemented strains on γ-GeSe in a range of −2% to 8% along the armchair, zigzag, and [110] directions. The *ab initial* molecular dynamics (AIMD) calculation was adopted to probe stability. As shown in Fig. S3 in the supplementary material, the geometric structure shows insignificant changes within 3 ps at 298 K at 8% strain along the [110] direction, indicating that γ-GeSe is capable of withstanding strains up to 8%. In Fig. 2(a), one can notice that the strain applied along the [110] direction changes the bond length of Ge–Se. The polarization intensity shows a similar trend under strain [Fig. 2(c)], indicating that the tensile force along the [110] direction leads to increment of polarization, while compression reduces polarization to 5.80×10^{-12} C/m. Notably, polarization reaches up to 1.77×10^{-11} C/m under 8% tensile strain along the [110] direction, similar to that of a typical 2D ferroelectric material MoS_2.[44] The trend of change is similar to the [110] direction strain, but the increase level of polarization intensity is lower than that of the [110] direction strain.

Since the off-centering displacements of Ge and Se atoms give rise to intrinsic polarization and generate a built-in electric field along the z direction, we present in Fig. 2(b) the differences in planar average potential between the upper and lower surfaces of γ-GeSe along the [110] direction strain. Notably, the magnitude of difference, Δϕ, varies with strain. Δϕ increases with tensile strain, reaching a maximum of 1.33 eV under 8% strain, which is ascribed to the increase in bond length caused by stretching, leading to the increase in the polarization intensity and the built-in electric field. The changes in the built-in electric field increase Δϕ. The planar average potential under the armchair and zigzag strain is shown in Figs. S4 and S5 in the supplementary material, where Δϕ under these two strains is smaller than that under the [110] direction strain, indicating that the [110] direction strain imposes more significant impact on the increase in polarization intensity.

To shed light on the principle of the generation of different electrostatic potentials, we calculated the charge differential density diagram (CDD), as shown in Fig. 2(d), where the upper layer of Ge atoms shows the electronic dissipation due to their electronegativity. Interestingly, as the tensile strain increases, the degree of electron dissipation gradually intensifies. The change of electron configuration leads to the generation of an internal electric field. In addition, the Bader charge population analysis was also conducted to quantitatively evaluate charge transfer under tensile stress. As the [110] direction strain increases, the Bader charge transfer increases gradually [Fig. 2(e)], which is similar to the trend of the polarization intensity and electrostatic potential change. The Bader charge is highest (0.585|e|) under the strain of 8%, indicating maximum polarization intensity and internal electric field strength. The charge transfer under the armchair or zigzag strain is not as significant as that under the [110] direction strain. The charge differential density along the zigzag and armchair directions is shown in Figs. S6 and S7in the supplementary material, indicating that the [110] direction strain is more effective in increasing the built-in electric field.

C. Electronic properties

The band structure of γ-GeSe calculated with the HSE06 method is shown in Fig. 3(a), where γ-GeSe monolayer is an indirect 2D semiconductor with a bandgap of 3.02 eV (close to 3.07 eV in other reports[27]), which is not suitable as a semiconductor catalyst because the large bandgap requires more energy to generate electron–hole pairs, leading to higher possibilities for recombination. This is also the reason why this material has been scarcely reported as a catalyst in previous studies. The valence band maximum (VBM) and conduction band minimum (CBM) are located between the G and M points, respectively.

Since the application of external strain has been proven to be a convenient method to regulate band structures of 2D materials, the influence of stain along armchair, zigzag, and [110] directions on the band structure of γ-GeSe is investigated, as shown in Fig. 3(b). The bandgap of γ-GeSe reduces with the increase of strain (1.97 eV under 8% strain along the [110] direction). The regulation effect of strain on bandgap under the [110] direction is more severe than that under armchair or zigzag directions. The PDOS (projected density of states) elucidates the reason of the bandgap modulation. CBM (conduction band minimum) is primarily influenced by the p-orbitals of Ge and Se atoms [Fig. S8 in the supplementary material]. With the application of strain, a significant leftward shift of the Ge p-orbital within the CBM occurs, thereby reduced the bandgap. The strain altered the crystal structure of γ-GeSe, thereby modifying its electronic structure and reducing the bandgap.

To investigtate the influence of built-in electric field on the movement of charge carrier, Table S2 in the supplementary material lists the effective mass of electrons in γ-GeSe under the [110]

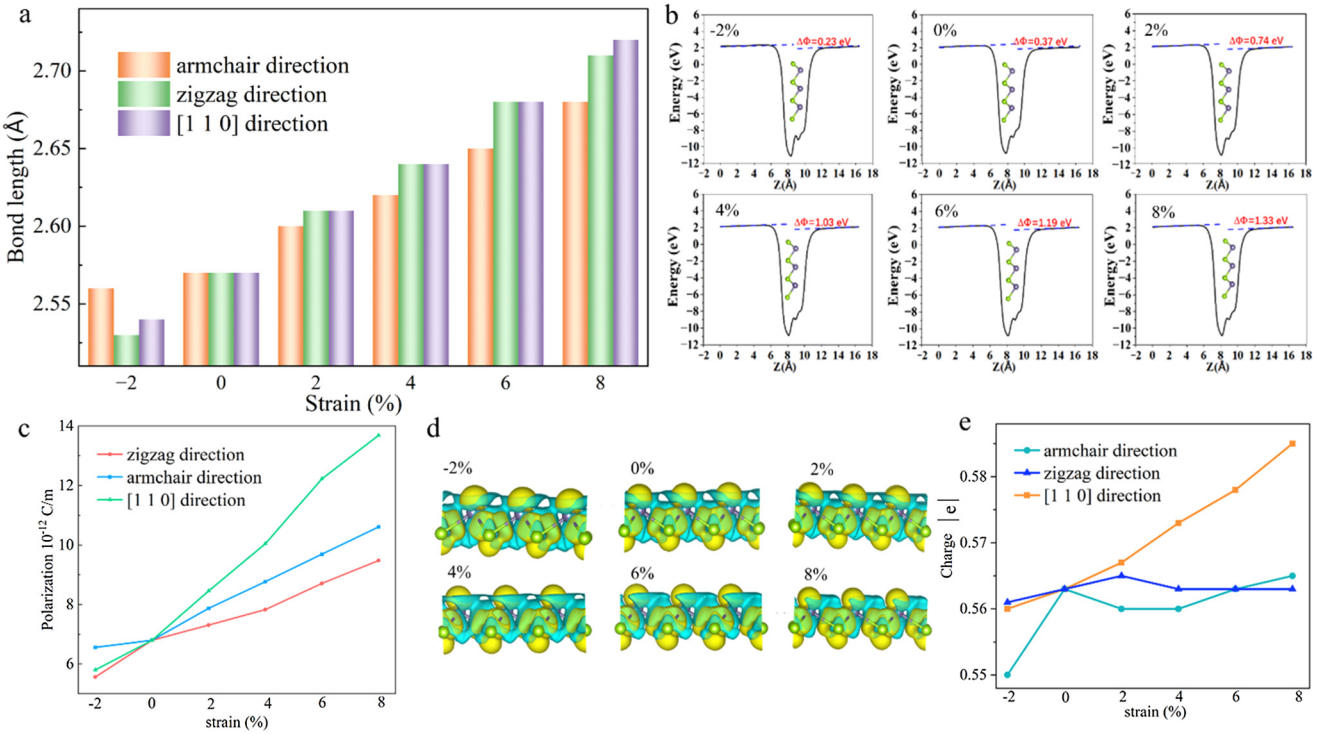

FIG. 2. Piezoelectric properties of GeSe. (a) The bond length under different strains. (b) Electrostatic potential of γ-GeSe along the Z axis under strain along the [110] direction. (c) The polarization intensity of γ-GeSe under [110] direction strain. (d) Differential charge density under strain along the [110] direction. The yellow isosurface indicates electron accumulation and the blue electron dissipation. (e) Analysis of the Bader charge under different strains.

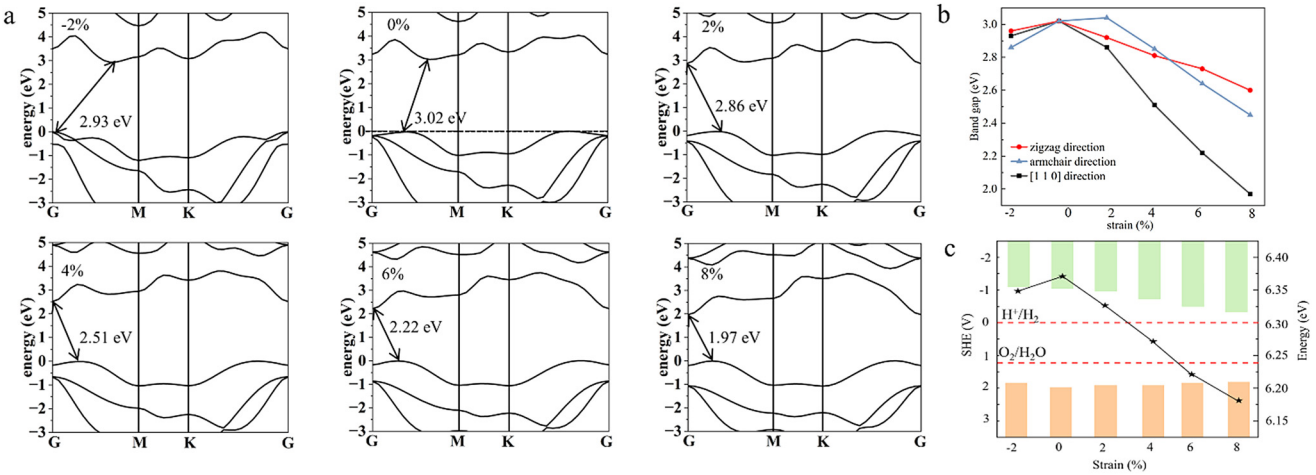

FIG. 3. Electronic structure of γ-GeSe. (a) Calculated band structure under strain along the [110] direction within the HSE06 method. (b) The bandgap under different strains. (c) The histogram diagram of redox potential and point line diagram of work function under [110] direction strain. The orange color represents oxidation potential and the green one reduction potential.

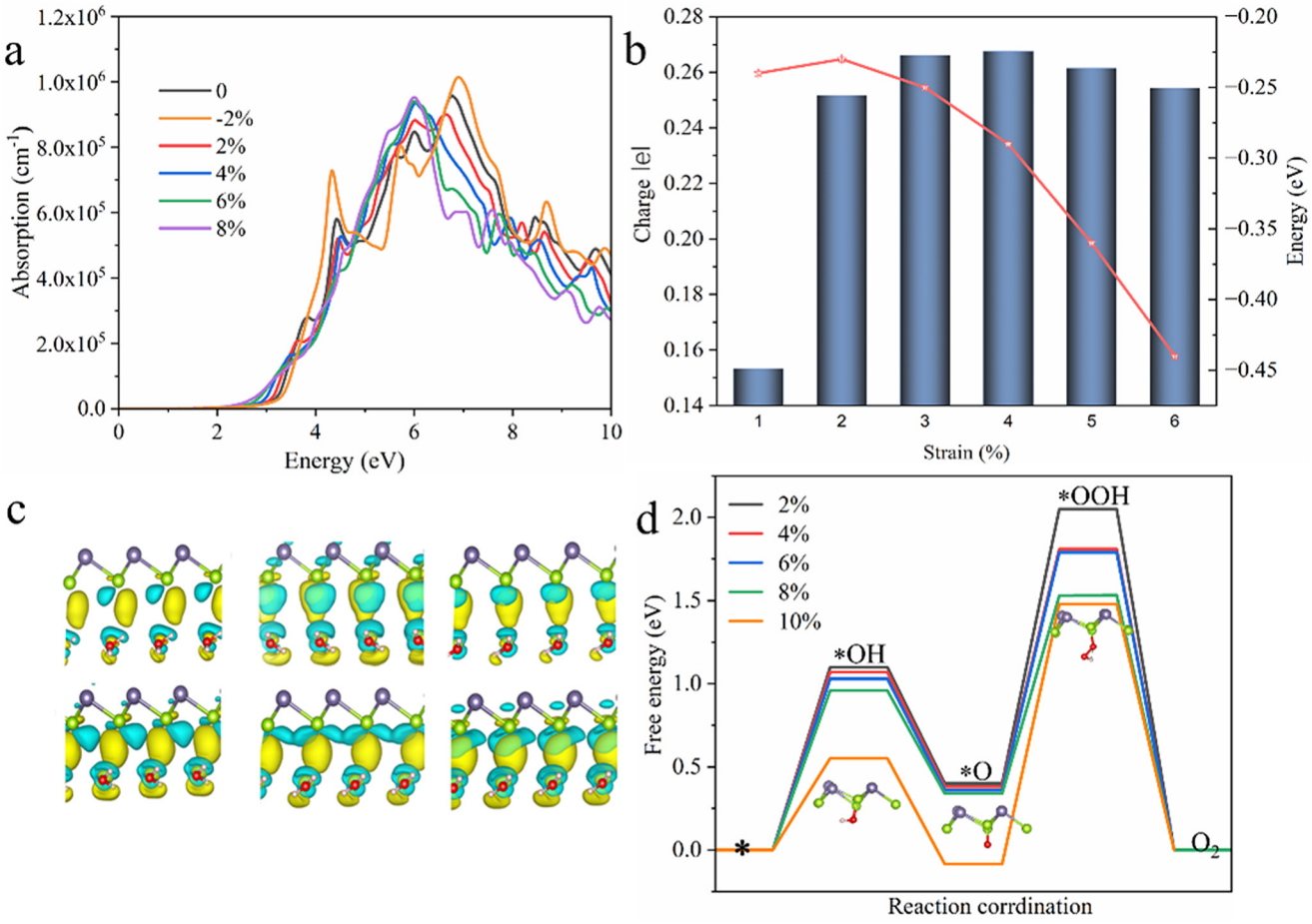

FIG. 4. Catalytic performance under strain. (a) Optical absorption of γ-GeSe under [110] direction strain. (b) The adsorption energy point of Se atoms adsorbing H_2O under strains and the Bader charge analysis diagram under [110] direction strain. (c) Charge differential density of γ-GeSe with adsorbed H_2O under [110] direction strain from −2% to 8%. The red and white spheres are O and H atoms, respectively. The yellow isosurface indicates electron accumulation and the blue one electron dissipation. (d) The Gibbs free energy of OER at Se adsorption sites under [110] direction strain.

direction strain. Under the tensile strain, the built-in electric field reduces the effective mass of electrons, thereby facilitating carrier transfer. Since the [110] direction strain induces the strongest built-in electric field and allows to significantly regulate electronic structures, we conducted further research of this strain effect. The band edge of γ-GeSe under different strain is aligned and compared with the potentials associated with hydrogen reduction and water oxidation reactions at pH = 0 [Fig. 3(c)]. γ-GeSe under strain along the [110] direction satisfies the oxidation–reduction potential, thereby holding promise as an excellent photocatalyst for water decomposition.

Figure 3(c) shows the plotted work function under strain, where one can see that both the tensile and compression reduce work function. The lowest work function takes place at 8% tensile. The magnitude of surface work function is intricately linked to the photoelectron emission, which denotes the generation of electrons on the surface of a material under illumination. A smaller work function facilitates a more facile photoelectron emission process, thereby enhancing the feasibility of achieving photocatalytic reaction. This finding implies that 8% strain holds the potential for enhancing photocatalytic efficiency, as reported previously showing that the catalytic efficiency is inversely proportional to work function.[45,46]

D. Optical properties

The optical absorption coefficient α(ω) of γ-GeSe is calculated by the HSE06 hybrid functional under different strains along the [110] direction. The optical absorption $\alpha(\omega)$ of the individual monolayer can be obtained as follows:[47]

$$\alpha(\omega) = \sqrt{2\omega}\sqrt{\sqrt{\varepsilon_1^2(\omega) + \varepsilon_2^2(\omega)} - \varepsilon_1(\omega)}, \quad (13)$$

where ε_1 and ε_2 represent the real and imaginary parts of the dielectric function, respectively. γ-GeSe under strain along the [110] direction shows significant optical absorption coefficients, as seen in Fig. 4(a), especially in the near-ultraviolet and visible light regions [Fig. S9 in the supplementary material]. In the visible region, the absorption coefficient exceeds $10^4\ cm^{-1}$, which is larger than those of the previously explored 2D materials,[48] indicating that γ-GeSe has excellent solar energy utilization efficiency and is suitable as a photocatalyst. Additionally, our findings reveal that tensile strain induces a redshift in the light absorption spectrum within the visible range, which is mainly attributed to the reduction in bandgap, indicating that tensile strain enhances light absorption properties of γ-GeSe.

E. Interfacial charge transfer and OER

Since the adsorption of water molecules is a prerequisite for the OER reaction, we calculated the water adsorption energy of GeSe under different strains as follows:

$$E_{ads} = E_{\gamma-GeSe+H_2O} - E_{\gamma-GeSe} - E_{H_2O}. \quad (14)$$

Our calculations indicate that strain induced built-in electric field is beneficial for adsorbing polar water molecules, and that the maximum strain of 8% leads to the most stable adsorption of water molecules [Fig. 4(b)]. Moreover, we calculated the charge differential density of γ-GeSe with adsorbed water molecules [Fig. 4(c)] and analyzed the interface charge transfer mechanism under different strains by Bader charge-population analysis. The increase of strain is beneficial for electron accumulation between γ-GeSe and H_2O molecules. The strain gives rise to the accumulation of interlayer electrons, indicating that the increased internal electric field imposes a positive effect on charge transfer at interfaces, consistent with the calculated results of electron effective mass. We have also calculated the Gibbs free energy diagram ($U = 0$, pH = 0) to depict the performance of the oxygen evolution reaction (OER). The OER consists of four successive steps [Fig. 4(d)]: (i) the initial deprotonation of H_2O molecules to yield OH, (ii) the subsequent deprotonation of OH upon interaction with another deprotonated H_2O molecule, generating the adsorbed oxygen (O), (iii) formation of OOH through the aforementioned process, and (iv) the deprotonation of OOH to generate an O_2 molecule, which subsequently detaches from the surface.

In this study, we examine the catalytic activity of OER under various tensile strains by evaluating the overpotential. Notably, it is observed that on the Se site, the rate-determining step corresponds to the formation of OOH, exhibiting a theoretical overpotential. The Gibbs free energy diagrams for other adsorption sites can be found in Fig. S11 in the supplementary material. As strain increases, the Gibbs free energy associated with the rate-determining step diminishes. Specifically, under 8% strain, the minimum step potential is reduced to 1.19 eV, surpassing the performance of other 2D materials utilized for OER, such as graphene.[49] An inverse correlation between strain magnitude and Gibbs free energy is observed, i.e., the higher strain levels correspond to lower Gibbs free energy. Subsequently, we calculated the oxygen evolution reaction step diagram under a larger strain of 10%, as depicted in Fig. 4(d) and Fig. S11 in the supplementary material. The calculations reveal that the optimal performance is achieved at 8% strain, suggesting that 8% strain is optimum for OER photocatalytic reaction. Based on the diagrams of the OER Gibbs free energy and the interface charge transfer mechanism, we conclude that the tensile strain increases the built-in electric field of γ-GeSe and that the driving force of built-in electric field separates charge carriers effectively, thereby promoting the photocatalytic OER reaction. The optimal performance is achieved at 8% strain.

IV. CONCLUSIONS

We have demonstrated that tensile strain can modulate polarization intensity, electronic structure, and optical absorption properties of γ-GeSe, resulting in significant improvement of OER performances. We explored the mechanism of the piezoelectric effect, illustrating that it functions by regulating the position of positive and negative charge centers to generate an internal electric field. The presence of this electric field facilitates the separation of electrons and holes, hence enhancing the process of OER. Furthermore, we have provided an explanation for the improvement in OER efficiency that can be attributed to changes in the electronic structure caused by the piezoelectric effect. The application of strain along the [110] direction amplifies the polarization intensity of γ-GeSe, enhances the built-in electric field, and promotes effective separation of photo-generated electron–hole pairs. We also find that strain modifies work function and bandgap of γ-GeSe, adjusts positions of valence band and conduction band edges to enhance their oxidation-reduction ability, and expands the light absorption range, leading to the improvement of photocatalytic performances. Further intensification of strain causes more pronounced interfacial charge transfer and progressively reduced rate-determining step of the Gibbs free energy, reaching a minimum of 1.19 eV at 8% strain along the [110] direction. The findings show that γ-GeSe holds promise as a 2D OER material under strain, and such a strategy of using a single piezoelectric material to generate internal electric fields for OER opens up a new avenue in developing novel highly efficient catalysts. Our research provides physical theoretical support for the application of the piezoelectric effect in OER and provides guidance for the use of piezoelectric materials in various fields.

SUPPLEMENTARY MATERIAL

See the supplementary material for the AIMD simulation process of γ-GeSe under 8% strain along the [110] direction at 298 K; electrostatic potential of γ-GeSe under strain along the armchair and zigzag directions; charge differential density diagram of γ-GeSe under strains along the armchair and zigzag directions; corresponding configurations and Gibbs free energies of γ-GeSe at Ge adsorption sites; elastic stiffness coefficients, relaxed-ion piezoelectric coefficients and electronic effective mass of γ-GeSe.

ACKNOWLEDGMENTS

This work was supported by the National Natural Science Foundation of China (No. U1803128), the Taishan Scholar Project (No. tsqn201909054), the Natural Science Foundation of Shandong

Province (No. ZR2022JQ22), the Fundamental Research Funds for the Central Universities to M.Q. (No. 202341006), and Xinjiang Tianchi Talents Project (No. 2023000043), and computational resources from the Center for High-Performance Computing and System Simulation, Pilot National Laboratory for Marine Science and Technology (Qingdao).

AUTHOR DECLARATIONS

Conflict of Interest

The authors have no conflicts to disclose.

Author Contributions

Tianqi Zhang: Writing – original draft (equal). **Long Zhou:** Writing – original draft (equal). **Guobo Chen:** Software (supporting). **Songrui Wei:** Methodology (supporting). **Rong Sun:** Writing – original draft (supporting). **Yunping Li:** Visualization (supporting). **Lijian Meng:** Visualization (supporting). **Guanglong Zhang:** Data curation (supporting). **Shuwei Xia:** Writing – original draft (equal). **Zhongchang Wang:** Writing – review & editing (equal). **Meng Qiu:** Writing – review & editing (equal).

DATA AVAILABILITY

The data that support the findings of this study are available from the corresponding authors upon reasonable request.

REFERENCES

[1]M. Wang, J. Ioccozia, L. Sun, C. Lin, and Z. Lin, "Inorganic-modified semiconductor TiO_2 nanotube arrays for photocatalysis," Energy Environ. Sci. **7**, 2182–2202 (2014).
[2]A. Fujishima and K. Honda, "Electrochemical photolysis of water at a semiconductor electrode," Nature **238**, 37–38 (1972).
[3]C. Xu, P. R. Anusuyadevi, C. Aymonier, R. Luque, and S. Marre, "Nanostructured materials for photocatalysis," Chem. Soc. Rev. **48**, 3868–3902 (2019).
[4]P. Zhou, I. A. Navid, Y. Ma, Y. Xiao, P. Wang, Z. Ye, B. Zhou, K. Sun, and Z. Mi, "Solar-to-hydrogen efficiency of more than 9% in photocatalytic water splitting," Nature **613**, 66–70 (2023).
[5]H. Wang, L. Zhang, Z. Chen, J. Hu, S. Li, Z. Wang, J. Liu, and X. Wang, "Semiconductor heterojunction photocatalysts: Design, construction, and photocatalytic performances," Chem. Soc. Rev. **43**, 5234–5244 (2014).
[6]Y. Li, C. Gao, R. Long, and Y. Xiong, "Photocatalyst design based on two-dimensional materials," Mater. Today Chem. **11**, 197–216 (2019).
[7]E. Pakizeh, M. Mohammadi, and A. Mostafaei, "Effect of hydrogen concentration on the structural, electronic and optical properties of 2D monolayer MXenes: DFT study," Solid State Commun. **369**, 115214 (2023).
[8]M. Mohammadi and E. Pakizeh, "Electronic structure, optical properties, and potential applications of n-BN/WS2 (n = 1 to 4) heterostructures," J. Electron. Mater. **50**, 4696–4704 (2021).
[9]E. Pakizeh, J. Jalilian, and M. Mohammadi, "Electronic, optical and thermoelectric properties of Fe_2 ZrP compound determined via first-principles calculations," RSC Adv. **9**, 25900–25911 (2019).
[10]T. Zhang, L. Zhou, G. Chen, S. Xia, and M. Qiu, "Theoretical study on an oxygen-modified phosphorene autogenous Z-scheme heterojunction for hydrogen evolution," Chem. Commun. **59**, 1517–1520 (2023).
[11]Z. Wang, J. Song, F. Gao, R. Su, D. Zhang, Y. Liu, C. Xu, X. Lou, and Y. Yang, "Developing a ferroelectric nanohybrid for enhanced photocatalysis," Chem. Commun. **53**, 7596–7599 (2017).
[12]A. Kakekhani and S. Ismail-Beigi, "Ferroelectric-based catalysis: Switchable surface chemistry," ACS Catal. **5**, 4537–4545 (2015).
[13]A. Kakekhani, S. Ismail-Beigi, and E. I. Altman, "Ferroelectrics: A pathway to switchable surface chemistry and catalysis," Surf. Sci. **650**, 302–316 (2016).
[14]J. Zhang, C. Wang, and C. Bowen, "Piezoelectric effects and electromechanical theories at the nanoscale," Nanoscale **6**, 13314–13327 (2014).
[15]Z. Liang, C.-F. Yan, S. Rtimi, and J. Bandara, "Piezoelectric materials for catalytic/photocatalytic removal of pollutants: Recent advances and outlook," Appl. Catal. B **241**, 256–269 (2019).
[16]J. Zhang, R. Sun, Y. Ge, J. Wang, Z. Wang, L. Meng, F. L. Deepak, M. Zhang, P. Yin, and F. Cheng, "Atomic-scale structure and nonlinear optical absorption of two-dimensional GeS," J. Mater. Sci. Technol. **187**, 188–194 (2024).
[17]K.-S. Hong, H. Xu, H. Konishi, and X. Li, "Direct water splitting through vibrating piezoelectric microfibers in water," J. Phys. Chem. Lett. **1**, 997–1002 (2010).
[18]J. Wu, N. Qin, and D. Bao, "Effective enhancement of piezocatalytic activity of $BaTiO_3$ nanowires under ultrasonic vibration," Nano Energy **45**, 44–51 (2018).
[19]H. Qiao, H. Liu, Z. Huang, R. Hu, Q. Ma, J. Zhong, and X. Qi, "Tunable electronic and optical properties of 2D monoelemental materials beyond graphene for promising applications," Energy Environ. Mater. **4**, 522–543 (2021).
[20]K. S. Novoselov, A. K. Geim, S. V. Morozov, D.-e. Jiang, Y. Zhang, S. V. Dubonos, I. V. Grigorieva, and A. A. Firsov, "Electric field effect in atomically thin carbon films," Science **306**, 666–669 (2004).
[21]D. Han, G. Yu, A. Liu, G. Li, W. Wang, B. He, Z. Hou, and H. Yin, "Soft-template-assisted synthesis of N-doping layered CoS_2 nanoparticles as an advanced anode for sodium-ion batteries," Carbon Lett. **33**, 1839–1846 (2023).
[22]T. Guo, Y. Zhou, Z. Wang, J. Cunha, C. Alves, P. Ferreira, Z. Hou, and H. Yin, "Indium nitride nanowires: Low redox potential anodes for lithium-Ion batteries," Adv. Sci. **11**, 2310166 (2024).
[23]F. Xia, H. Wang, D. Xiao, M. Dubey, and A. Ramasubramaniam, "Two-dimensional material nanophotonics," Nat. Photonics **8**, 899–907 (2014).
[24]J. Low, S. Cao, J. Yu, and S. Wageh, "Two-dimensional layered composite photocatalysts," Chem. Commun. **50**, 10768–10777 (2014).
[25]X. Li, J. Yu, and M. Jaroniec, "Hierarchical photocatalysts," Chem. Soc. Rev. **45**, 2603–2636 (2016).
[26]H. Arkın and E. Aktürk, "Investigation of adatom adsorption on single layer buckled germanium selenide," Appl. Surf. Sci. **390**, 185–189 (2016).
[27]C. Liu, S. Guan, H. Yin, W. Wan, Y. Wang, and Y. Zhang, "γ-geSe: A two-dimensional ferroelectric material with doping-induced ferromagnetism," Appl. Phys. Lett. **115**, 252904 (2019).
[28]W. Wu and Z. L. Wang, "Piezotronics and piezo-phototronics for adaptive electronics and optoelectronics," Nat. Rev. Mater. **1**, 1–17 (2016).
[29]W. Wu and Z. L. Wang, "Piezotronics and piezo-phototronics for adaptive electronics and optoelectronics," Nat. Rev. Mater. **1**, 16031 (2016).
[30]L. Pan, S. Sun, Y. Chen, P. Wang, J. Wang, X. Zhang, J. J. Zou, and Z. L. Wang, "Advances in piezo-phototronic effect enhanced photocatalysis and photoelectrocatalysis," Adv. Energy Mater. **10**, 2000214 (2020).
[31]F. Yang, P. Wang, J. Hao, J. Qu, Y. Cai, X. Yang, C. M. Li, and J. Hu, "Ultrasound-assisted piezoelectric photocatalysis: An effective strategy for enhancing hydrogen evolution from water splitting," Nano Energy **118**, 108993 (2023).
[32]G. Kresse and J. Furthmüller, "Efficient iterative schemes for *ab initio* total-energy calculations using a plane-wave basis set," Phys. Rev. B **54**, 11169 (1996).
[33]J. P. Perdew, K. Burke, and M. Ernzerhof, "Generalized gradient approximation made simple," Phys. Rev. Lett. **77**, 3865 (1996).
[34]J. Heyd, G. E. Scuseria, and M. Ernzerhof, "Hybrid functionals based on a screened Coulomb potential," J. Chem. Phys. **118**, 8207–8215 (2003).
[35]A. V. Krukau, O. A. Vydrov, A. F. Izmaylov, and G. E. Scuseria, "Influence of the exchange screening parameter on the performance of screened hybrid functionals," J. Chem. Phys. **125**, 224106 (2006).
[36]R. D. King-Smith and D. Vanderbilt, "Theory of polarization of crystalline solids," Phys. Rev. B **47**, 1651 (1993).
[37]D. Vanderbilt, "Berry-phase theory of proper piezoelectric response," J. Phys. Chem. Solids **61**, 147–151 (2000).

[38]Y. Zhang, T. Ouyang, C. He, J. Li, and C. Tang, "Monolayer group-V binary compounds ψ-BiP and ψ-SbP with ultrahigh piezoelectricity and stability," Phys. Rev. Mater. **7**, 016001 (2023).
[39]F. Li, T. Shen, C. Wang, Y. Zhang, J. Qi, and H. Zhang, "Recent advances in strain-induced piezoelectric and piezoresistive effect-engineered 2D semiconductors for adaptive electronics and optoelectronics," Nano-Micro Lett. **12**, 1–44 (2020).
[40]Á. Valdés, Z.-W. Qu, G.-J. Kroes, J. Rossmeisl, and J. K. Nørskov, "Oxidation and photo-oxidation of water on TiO_2 surface," J. Phys. Chem. C **112**, 9872–9879 (2008).
[41]Y. Zhou, M. Zhao, Z. W. Chen, X. M. Shi, and Q. Jiang, "Potential application of 2D monolayer β-GeSe as an anode material in Na/K ion batteries," Phys. Chem. Chem. Phys. **20**, 30290–30296 (2018).
[42]Y. Dai, X. Zhang, Y. Cui, M. Li, Y. Luo, F. Jiang, R. Zhao, and Y. Huang, "Theoretical insights into strong intrinsic piezoelectricity of blue-phosphorus-like group-IV monochalcogenides," Nano Res. **15**, 209–216 (2022).
[43]S. Bertolazzi, J. Brivio, and A. Kis, "Stretching and breaking of ultrathin MoS_2," ACS Nano **5**, 9703–9709 (2011).
[44]P. Meng, Y. Wu, R. Bian, E. Pan, B. Dong, X. Zhao, J. Chen, L. Wu, Y. Sun, Q. Fu, Q. Liu, D. Shi, Q. Zhang, Y. W. Zhang, Z. Liu, and F. Liu, "Sliding induced multiple polarization states in two-dimensional ferroelectrics," Nat. Commun. **13**, 7696 (2022).
[45]F. Opoku, K. K. Govender, C. G. C. E. van Sittert, and P. P. Govender, "Role of MoS_2 and WS_2 monolayers on photocatalytic hydrogen production and the pollutant degradation of monoclinic $BiVO_4$: A first-principles study," New J. Chem. **41**, 11701–11713 (2017).
[46]S. H. Mir, S. Chakraborty, J. Wärnå, S. Narayan, P. C. Jha, P. K. Jha, and R. Ahuja, "A comparative study of hydrogen evolution reaction on pseudo-monolayer WS_2 and PtS_2: Insights based on the density functional theory," Catal. Sci. Technol. **7**, 687–692 (2017).
[47]S. Saha, T. Sinha, and A. Mookerjee, "Electronic structure, chemical bonding, and optical properties of paraelectric $BaTiO_3$," Phys. Rev. B **62**, 8828 (2000).
[48]Q.-K. Yin, C.-L. Yang, M.-S. Wang, and X.-G. Ma, "Two-dimensional heterostructures of AuSe/SnS for the photocatalytic hydrogen evolution reaction with a Z-scheme," J. Mater. Chem. C **9**, 12231–12238 (2021).
[49]C. Li, G. Yu, X. Shen, Y. Li, and W. Chen, "Theoretical study on the high HER/OER electrocatalytic activities of 2D GeSi, SnSi, and SnGe monolayers and further improvement by imposing biaxial strain or doping heteroatoms," Molecules **27**, 5092 (2022).